Identification and classification of very low frequency waves on a coral reef flat

Gawehn, M.; van Dongeren, AR; van Rooijen, Arnold; Storlazzi, C.D.; Cheriton, O.M.; Reniers, Ad

DOI
10.1002/2016JC011834

Publication date
2016

Document Version
Final published version

Published in
Journal Of Geophysical Research-Oceans

AGU PUBLICATIONS

JGR

Journal of Geophysical Research: Oceans

RESEARCH ARTICLE

10.1002/2016JC011834

Identification and classification of very low frequency waves on a coral reef flat

Matthijs Gawehn[1,2], Ap van Dongeren[1], Arnold van Rooijen[1,3], Curt D. Storlazzi[4], Olivia M. Cheriton[4], and Ad Reniers[1,2]

[1]Department of Applied Morphodynamics, Unit of Marine and Coastal Systems, Deltares, Delft, Netherlands, [2]Faculty of Civil Engineering and Geosciences, Delft University of Technology, Delft, Netherlands, [3]School of Earth & Environment and UWA Oceans Institute, University of Western Australia, Crawley Western Australia, Australia, [4]Pacific Coastal and Marine Science Center, U.S. Geological Survey, Santa Cruz, California, USA

Key Points:
- Very low frequency (0.001–0.005 Hz) waves on a reef flat can be categorized into four classes
- A new method identifies very low frequency wave resonance that occurred with high water levels and long incident wave periods
- Maximum nearshore very low frequency wave heights and observed flooding were driven by resonance

Supporting Information:
- Supporting Information S1

Correspondence to:
M. A. Gawehn,
Matthijs.Gawehn@deltares.nl

Citation:
Gawehn, M., A. van Dongeren, A. van Rooijen, C. D. Storlazzi, O. M. Cheriton, and A. Reniers (2016), Identification and classification of very low frequency waves on a coral reef flat, *J. Geophys. Res. Oceans*, *121*, 7560–7574, doi:10.1002/2016JC011834.

Received 24 MAR 2016
Accepted 14 SEP 2016
Accepted article online 19 SEP 2016
Published online 18 OCT 2016

Abstract Very low frequency (VLF, 0.001–0.005 Hz) waves are important drivers of flooding of low-lying coral reef-islands. In particular, VLF wave resonance is known to drive large wave runup and subsequent overwash. Using a 5 month data set of water levels and waves collected along a cross-reef transect on Roi-Namur Island in the Republic of the Marshall Islands, the observed VLF motions were categorized into four different classes: (1) resonant, (2) (nonresonant) standing, (3) progressive-growing, and (4) progressive-dissipative waves. Each VLF class is set by the reef flat water depth and, in the case of resonance, the incident-band offshore wave period. Using an improved method to identify VLF wave resonance, we find that VLF wave resonance caused prolonged (∼0.5–6.0 h), large-amplitude water surface oscillations at the inner reef flat ranging in wave height from 0.14 to 0.83 m. It was induced by relatively long-period, grouped, incident-band waves, and occurred under both storm and nonstorm conditions. Moreover, observed resonant VLF waves had nonlinear, bore-like wave shapes, which likely have a larger impact on the shoreline than regular, sinusoidal waveforms. As an alternative technique to the commonly used Fast Fourier Transformation, we propose the Hilbert-Huang Transformation that is more computationally expensive but can capture the wave shape more accurately. This research demonstrates that understanding VLF waves on reef flats is important for evaluating coastal flooding hazards.

1. Introduction

Fringing and atoll coral reefs front many tropical islands and are characterized by a steep fore reef, leading up to a reef crest, followed by a mildly sloping or horizontal reef flat to the island's shore. These reefs host complex and valuable ecosystems that support abundant marine species and provide resources for fisheries, recreation, and even building materials. An important function of these reefs is the protection of coastlines from coastal storm damage and flooding by reducing high-frequency wave energy up to 98% [*Ferrario et al.*, 2014]. However, particularly during storm and large swell conditions, overwash and coastal flooding may still occur [*Jaffe and Richmond*, 1992; *Hoeke et al.*, 2013] due to high water levels [*Vetter et al.*, 2010; *Quataert et al.*, 2015] and/or low-frequency wave resonance [*Péquignet et al.*, 2009; *Shimozono et al.*, 2015]. The combination of wave-induced setup, very low frequency (VLF, 0.001–0.005 Hz) motions and the propagation of infragravity (IG, 0.005–0.04 Hz) and high-frequency incident-band (HF, 0.04–0.2 Hz) waves can drive wave runup events that result in coastal flooding [*Merrifield et al.*, 2014; *Cheriton et al.*, 2016]. This not only poses a direct threat to coastal inhabitants, but can cause damage to infrastructure and can salinize scarce drinking water supplies in shallow aquifers and drinking water reservoirs [*Terry and Falkland*, 2011]. We denote VLF and IG waves collectively as low-frequency (LF, 0.001–0.04 Hz) waves.

On reefs, HF sea-swell waves start to break in a narrow surf zone close to the reef crest. In this process, they exert a force on the water column [*Longuet-Higgins and Stewart*, 1964; *Gourlay*, 1996b]; this force is balanced by a pressure gradient, which causes wave-induced setup that has been observed to be as high as, e.g., 0.5 m [*Munk and Sargent*, 1948] and 1.3 m [*Vetter et al.*, 2010], which is larger than setup typically observed on sandy beaches. Setup is a function of the incoming wave height [*Seelig*, 1983; *Vetter et al.*, 2010; *Quataert et al.*, 2015] and period [*Gerritsen*, 1980; *Gourlay*, 1996a; *Hench et al.*, 2008; *Nwogu and Demirbilek*, 2010], is tidally dependent [*Becker et al.*, 2014], and increases with decreasing offshore tidal water levels [*Seelig*, 1983].

In the zone of wave breaking, the energy in the HF band is also transferred to higher and lower wave frequencies [*Gerritsen*, 1980], causing wave spectra to become bimodal [*Young*, 1989; *Hardy and Young*, 1991]. For a fringing reef with a fore reef slope of approximately1:20, *Pomeroy et al*. [2012a] showed that IG waves were generated by the moving breakpoint mechanism, which is consistent with theory concerning steep slope regimes [*Symonds et al*., 1982; *Battjes et al*., 2004; *Baldock*, 2012]. After breaking, HF waves will further attenuate due to bottom friction dissipation on the reef flat [*Lowe et al*., 2005]. Bottom friction dissipation on the reef flat also dampens LF waves, but to a lesser extent than the HF waves [*Pomeroy et al*., 2012a]. This attenuation is controlled by wave shape, local hydrodynamic roughness, water depth, and the width of the reef flat [*Péquignet et al*., 2009; *Pomeroy et al*., 2012b]. At smaller water depths, this results in progressive-dissipative LF waves dominating the observed spectra [*Hardy and Young*, 1996; *Pomeroy et al*., 2012a; *Cheriton et al*., 2016]. However, at larger water depths, LF waves may reflect back from the shoreline, increasing the possibility of standing and even resonating LF oscillations.

Standing waves can be resonantly excited [*Lugo-Fernández et al*., 1998; *Pomeroy et al*., 2012b] by wave groups with a forcing period that corresponds to one of the natural reef-frequencies or eigenmodes [*Péquignet et al*., 2009; *Nwogu and Demirbilek*, 2010; *Shimozono et al*., 2015]. Eigenmode oscillations are known as seiching [*Rabinovich*, 2009] and can be approximated using open basin theory [*Wilson*, 1953]:

$$f_{n,th} = \frac{(2n+1)\sqrt{gh}}{4L} \quad for \;\; n=0,1,\ldots N \tag{1}$$

where n is mode number, g is gravitational acceleration, h is water depth, and L = length of the basin (in this case, width of the reef flat). Reef flats are typically too dissipative to accommodate LF resonance at higher modes, i.e., the flats are either too wide and/or the water too shallow; therefore, resonance is mostly observed for the longest fundamental mode (equation (1) with $n = 0$). This mode has a water level node near the reef crest and an antinode at the shoreline, meaning that a quarter wavelength matches the width of the reef flat [*Lugo-Fernández et al*., 1998].

We will differentiate between VLF and IG waves because resonance at the fundamental mode is typically associated with time scales of several minutes [*Lugo-Fernández et al*., 1998], which is in the VLF range. *Péquignet et al*. [2009] demonstrated that resonance at the fundamental mode significantly increased the amount of VLF energy reaching the shoreline during storm conditions at Ipan Reef in Guam. These motions possibly contributed to the inundation of parts of the island. Laboratory experiments conducted by *Nakaza and Hino* [1991] revealed that increased amplitude modulation of incoming short wave groups increased the amplitude of resonating waves. Moreover, the impact of seiches on a coastline may be further increased by an irregular wave shape: time-lapse photographs taken during the approach of a typhoon in 1987 at Okinawa showed a wave bore, comparable to a tsunami [*Nakaza et al*., 1990]. This is consistent with laboratory observations by *Nwogu and Demirbilek* [2010] and is caused by the nonlinear effects of advection and bottom friction that deform resonantly generated VLF waves into bore-like surges [*Nakaza and Hino*, 1991]. Video footage taken during Typhoon Haiyan in 2013 captured the destruction caused to a small Philippine town by a large, fast moving bore, which was subsequently modeled numerically by *Roeber and Bricker* [2015]. Due to the high propagation speed, the inertial forces at the front of such bores have the potential to transport boulders far inland [*Kennedy et al*., 2016] or cause severe damage to buildings [*Pistrika and Jonkman*, 2009]. *Roeber and Bricker* [2015] showed that the observed bore and its impact would have been even larger if the bore and reef resonance frequency had been a closer match. Hence, it is essential to understand VLF motion on reefs because, under certain conditions, they can exhibit large amplitudes and bore-like shapes at the shoreline, two factors that can contribute to coastal flooding and flood-related impact and damage.

In this study, we categorize VLF waves into four classes based on their physical behavior: resonant, standing (nonresonant), progressive-growing, and progressive-dissipative. In order to identify resonant cases, we present an approach based on a resonance diagram [*Nakaza and Hino*, 1991]. Our new method can be used as a simple tool to find resonance events in large data sets. Last, we show that resonant VLF waves at our study site occasionally display nonlinear, bore-like behavior, and propose an alternative method to the Fast Fourier Transformation (FFT) to capture complex VLF bore shapes in time series data.

In section 2, the field site and data processing are described. Then, the methods used to separate VLF wave classes are presented in section 3 and the results in section 4. In section 5, we elaborate on the detection

and appearance of the resonance phenomenon and the correlation between VLF wave classes and flooding. Finally, we summarize our findings in section 6.

2. Field Site and Data Processing

Roi-Namur is an atoll islet at the northern tip of Kwajalein Atoll, in the Republic of the Marshall Islands (Pacific Ocean, see Figure 1a). The islet is one of multiple study cases within the U.S. Strategic Environmental Research and Development Program (SERDP), where instruments have been deployed to collect field data for an extensive investigation on the vulnerability of low-lying islands to rising sea levels. Large wave events coinciding with high tidal levels have caused flooding of Roi-Namur in 2008 [*Hoeke et al*., 2013] and in 2014 [*Quataert et al*., 2015; *Cheriton et al*., 2016]. *Becker et al*. [2014] found that wave-induced setup at the island was tidally dependent and could be significant during a combination of low tide and energetic wave conditions. *Merrifield et al*. [2014] confirmed the potential of the area for extreme water levels and stressed the importance of LF wave variability and *Cheriton et al*. [2016] demonstrated that offshore water levels and LF waves were the primary drivers of the 2014 overwash event. In addition, *Cheriton et al*. [2016] suggested the frequent occurrence of resonance, especially for VLF wave periods at the fundamental mode of the reef. In this context, the data collected at Roi-Namur are ideal for a comprehensive investigation on VLF wave dynamics due to the large number of time records (3800 hourly bursts) that are long enough (34 min at 2 Hz) to resolve the VLF scales.

The fringing reef at the study site is characterized by a fore reef that commences at a depth of approximately 20 m with a lower, steeper section (slope ∼1:6) that merges at a depth of 10 m with an upper, milder sloped (∼1:15) section (Figure 1b). The fore reef is about 180 m wide and has a relatively rough surface due to the presence of corals. The nearly horizontal (slope ∼1:700) reef flat is characterized by a coral-algal pavement with sparsely scattered carbonate cobbles and boulders, and is, therefore, relatively smooth. The reef flat extends approximately 270 m and is bordered by a narrow sandy beach with a 1:6 slope.

Between 3 November 2013 and 13 April 2014, an array of four bottom-mounted pressure sensors, at sites defined as "fore," "outer," "mid," and "inner" (Figure 1b), recorded the pressure for 34 min every hour at 2 Hz. We refer to *Cheriton et al*. [2016] for greater detail on the instrumentation and sampling schemes. Pressure data were converted to pressure head [*Fofonoff and Millard*, 1983] and then corrected for the dynamic pressure by means of the pressure response factor [*Dean and Dalrymple*, 1991]. This procedure assumes linear wave theory and does not account for the effects of tidal or wind-driven currents due to the lack of velocity measurements. Spectral parameters were retrieved from smoothed, one-dimensional spectra of the demeaned and detrended burst signal. Hanning windows were applied to time segments of 17 min with 50% overlap, yielding a spectral bandwidth of 0.001 Hz. To overcome imprecisions caused by occasionally bimodal fore reef spectra, fore reef peak periods were obtained from smoother spectra by partitioning each time series into 4 min segments with 50% overlap.

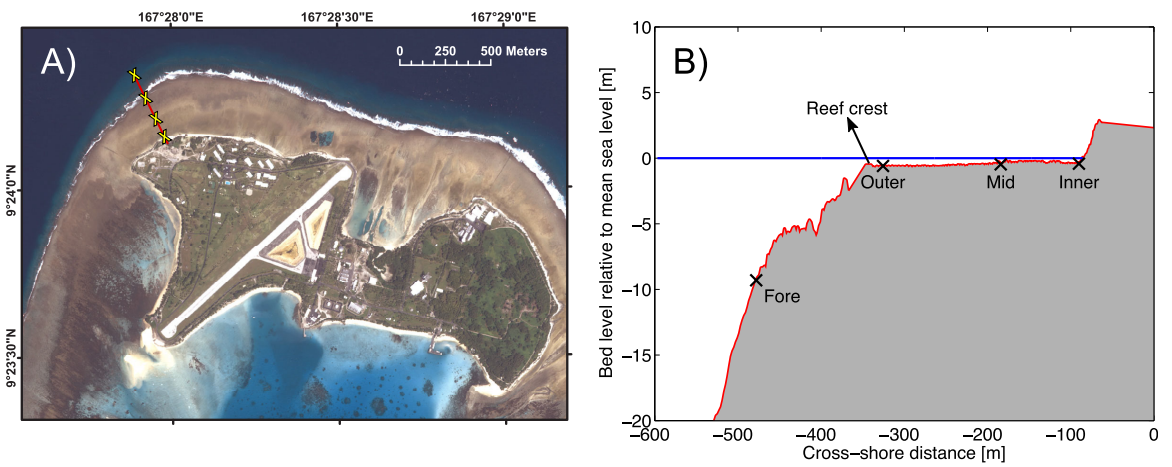

Figure 1. Views of the study area on Kwajalein Atoll in the Republic of the Marshall Islands. (a) Map view of the field site on Roi-Namur Island, with the location of the instruments denoted by "cross" along the cross-reef transect; (b) bathymetric profile of the cross-reef transect and location of the pressure sensors.

Over the 5 month deployment, significant wave heights measured on the fore reef station ($H_{s,fore}$) ranged from 0.7 to 3.8 m and peak periods (T_p) from 5 to 19.6 s. The highest VLF wave energy was measured in the vicinity of the shoreline at the inner reef flat. There, VLF significant wave heights ($H_{s,VLF,inner}$) exceeded 0.4 m 5% of the records, with a maximum of 0.86 m in the early morning hours of 3 March 2014. The days of 2–3 March coincided with an energetic wave event that caused overwash of the beach berm and partial flooding of the island [*Quataert et al*., 2015; *Cheriton et al*., 2016]. These reported wave parameters are slightly different from *Cheriton et al*. [2016] because we used the fore reef station as the offshore reference station and increased the VLF range from 0.001–0.004 to 0.001–0.005 Hz so that it is symmetrically defined around the average spectral peak measured on the inner reef flat.

3. Methodology

3.1. Very Low Frequency Wave Classification

The inner reef flat VLF wave energy was normalized to incident (HF) wave energy at the fore reef and ordered according to fore reef HF wave peak frequency and the corresponding spatially averaged (across all reef flat stations) reef flat water depth (h) (Figure 2). As the offshore wave frequency decreases and the reef flat water depth increases, the amount of normalized VLF energy at the inner reef flat increases (Figure 2). By applying a selection process with three criteria, we can identify and classify VLF waves with similar behavior (Figure 3). The selection process produces four classes of VLF motions on the reef flat: resonant, standing (nonresonant), progressive-growing, and progressive-dissipative waves. Next we describe the selection process in detail.

3.2. Resonance Criterion

Resonant waves were found using a resonance diagram (Figure 4), which visualizes the natural response of a forced system to various forcing frequencies and typically shows a peak when the forcing frequency corresponds to an eigenmode of the system. Here the reef flat is the system, which is forced by wave groups of different frequencies and has theoretical eigenmodes at $f_{n,th}$ (equation (1)). Wave group frequencies are determined by the spectrum of the wave group envelope $A(t)$ at the fore reef, which is obtained by a Hilbert transform following the approach by *Van Dongeren et al*. [2003]. The importance of various forcing frequencies is determined by quantifying the energy transfer between the incident wave group envelope spectrum and the inner reef flat wave spectrum through the use of a transfer function [*Emery and Thomson*, 2001; *Péquignet et al*., 2009; *Harkins and Briggs*, 1994; *Pomeroy et al*., 2012b]:

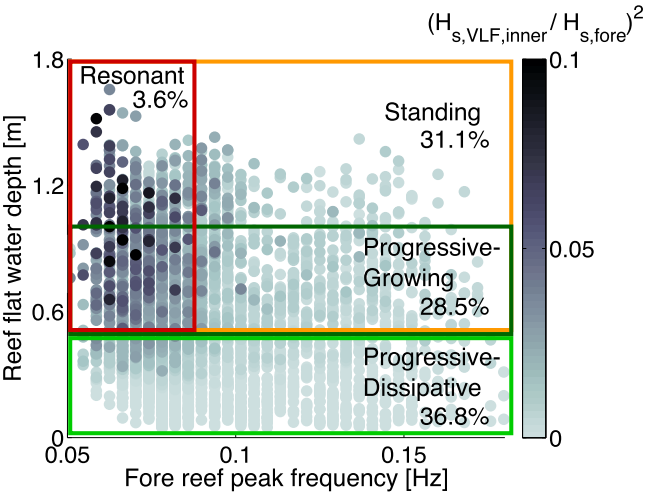

Figure 2. Normalized very low frequency (VLF) energy $(H_{s,VLF,inner}/H_{s,fore})^2$ at the inner reef flat as a function of the fore reef incident wave peak frequency and time-averaged and spatially averaged reef flat water depth. Normalized VLF energy levels are indicated by the gray color scale. The four major VLF wave classes are distinguished by the colored boxes, and the percentage of occurrence is listed for each.

$$H_{Ay}(f) = \frac{|G_{Ay}(f)|}{G_{AA}(f)} \quad (2)$$

where $H_{Ay}(f)$ is the energy transfer at frequency f; $G_{Ay}(f)$ is the cross spectrum between the fore reef envelope (i.e., the forcing) and the inner reef flat wave record; and $G_{AA}(f)$ is the auto-spectrum of the envelope signal $A(t)$. The frequency at which the energy transfer peaks is treated as potential resonance frequency ($f_{p,transfer}$). The closer $f_{p,transfer}$ is to an eigenmode $f_{n,th}$, the higher the expected response, which we express by the normalized inner reef flat energy ($normE_{p,transfer}$) at $f_{p,transfer}$. Here we normalized the variance at $f_{p,transfer}$ on the inner reef flat by the variance of $A(t)$ at the fore reef station. VLF resonance occurs at the fundamental mode $f_{0,th}$ (equation (1); $n = 0$), hence, the peak of the

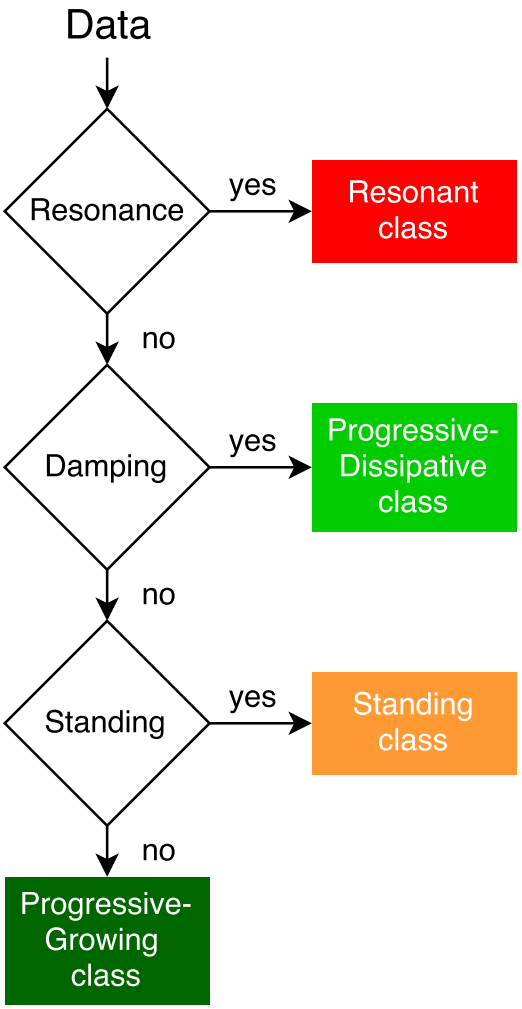

Figure 3. Decision tree used to identify the different very low frequency (VLF) wave classes. The colors correspond to the boxes in Figure 2.

resonance diagram around $f_{p,transfer}/f_{0,th} = 1$ is chosen as the collection of resonance events, using a minimum threshold value for $normE_{p,transfer}$. However, choosing an appropriate threshold value is not straightforward. We used a sensitivity analysis to identify this threshold, the details of which are described in section 5.

Pomeroy et al. [2012b] applied a different method to identify resonance. This method utilizes wave measurements from two sites on a reef flat, and identifies instances when three criteria are met: (1) a high coherence, (2) a phase difference closely correspondent to 0° or 180°, and (3) an increasing amplitude toward the coastline. As these criteria are met for both resonant conditions and nonresonant standing waves with an antinode at the shoreline and a node near the reef crest, this method has the potential to incorrectly identify nonresonant standing waves as resonant. Therefore, we use the resonance diagram to identify resonance separately and the "three criteria method" by *Pomeroy et al.* [2012b] to distinguish standing wave conditions from the remaining events. The performance of both methods is discussed in section 5.

3.3. Damping Criterion

VLF waves that are not identified as resonance events are then evaluated for damping (Figure 3) by looking for a decrease of $H_{s,VLF}$ from the outer to the inner reef flat sites. If $H_{s,VLF}$ decreases over the reef flat, standing waves are not expected and the VLF wave is labeled as "progressive-dissipative" (Figure 3). Note that the damping criterion does not act on individual harmonics but the bulk value $H_{s,VLF}$.

3.4. Standing Wave Criterion

The remaining VLF waves include those with increasing or constant $H_{s,VLF}$ over the reef flat, such as progressive-growing or standing waves. Standing VLF waves were detected by means of the coherence, phase difference, and amplification criteria described above [*Pomeroy et al.*, 2012b]. If these criteria are met, a VLF wave is classified as a standing wave; if not, it is classified as a progressive-growing VLF motion (Figure 3). Note that we chose to apply these criteria to the mid and inner reef flat sites since the outer reef flat gauge was located in a region where waves were still breaking, which results in inaccuracies when using the phase difference criterion.

3.5. Cross-Correlation Analysis

The nature of the different wave classes are illustrated by the respective energy spectra on the reef and the cross correlation of the fore reef wave group envelope with the VLF band-pass filtered time series of the reef flat stations. Following *Janssen et al.* [2003],

$$R_{\eta A}(\tau) = \frac{\langle \eta_{VLF}(t) A(t+\tau) \rangle}{\sigma_\eta \sigma_A} \tag{3}$$

where $R_{\eta A}(\tau)$ are the cross-correlation results between the fore reef envelope signal $A(t)$ and the VLF-band passed surface elevation $\eta_{VLF}(k)$ at reef station $k = \{inner, mid, outer, fore\}$. Each $R_{\eta A}(\tau)$ represents an array of

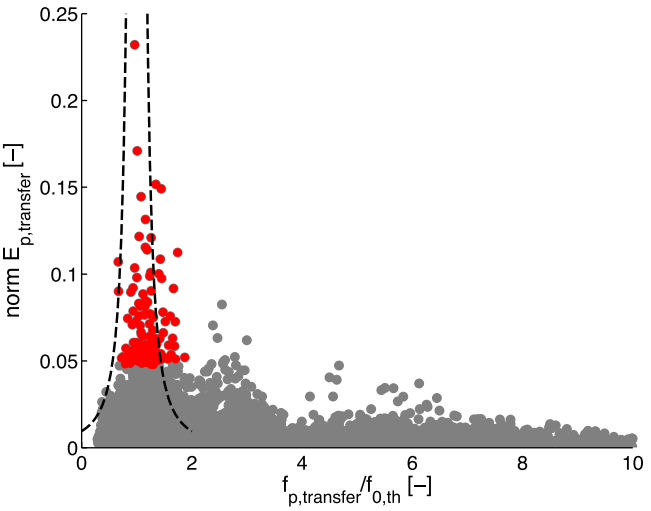

Figure 4. Distribution of bursts as a function of the normalized inner reef flat energy at the peak transfer frequency $f_{p,transfer}$ and the ratio of $f_{p,transfer}$ over the theoretical fundamental frequency $f_{0,th}$. The identified very low frequency (VLF) resonance events are highlighted in red. The analytical solution for a harmonically forced, undamped system is superimposed on the scatter as reference (black dashes). Bursts with dominant group frequencies near $f_{0,th}$ cluster around the unity value and validate the open basin idealization for this reef. Resonance at higher modes is also apparent, but damped compared to the fundamental mode.

cross-correlation values at different time-lags τ. The time-lag τ indicates the shift of signals and in this case ranges from -500 to 500 s, $\langle \ldots \rangle$ denotes the time averaging operator, σ the standard deviation, and resulting cross correlations have the range $-1 \leq R_{\eta A} \leq 1$.

4. Results

4.1. Resonant Waves

The results of the selection process show that resonant VLF waves occurred over the Roi-Namur reef flat 3.6% of the records (Figure 5a). Generally, these resonant VLF motions occurred with larger water depths (h) on the reef flat $h = 0.4$–1.6 m (described by a normal distribution with mean $\mu = 0.9$ m and standard deviation $\sigma = 0.2$ m), see also Figures in Supporting information S1 for the distribution of the data and relatively long incident peak periods ($T_p = 11$–19 s; normal distribution; $\mu = 15$ s; $\sigma = 2$s) (Figure 2). During these resonance events, the VLF energy at the inner reef flat was high (Figure 5b; red curve), with up to 16% ($\mu = 5\%$) of the fore reef HF wave energy being transferred to the narrow VLF band on the inner reef flat, compared to the overall average of 1%.These percentages are computed as the ratio of inner reef flat VLF energy over total fore reef energy (Figures 5b, 5e, 5h, and 5k; green curve). For reference, the ratios of HF energy on the fore reef over IG and HF energy on the inner reef flat reached up to 10% ($\mu = 4\%$) and 3% ($\mu = 1\%$), respectively, for this class. For the generation of resonance over the reef flat, incident HF wave heights were less important than incident wave peak periods, as resonance occurred across a range of fore reef wave heights ($H_s = 0.8$–3.4 m). Wave events that had both large wave heights and relatively long periods drove elevated setup over the reef flat, which resulted in sufficient water depths for VLF resonance to occur under low tide conditions (e.g., on 2 March 2014 resonance occurred with MSL -0.7 m, $H_s = 3.4$ m, $T_p = 15$ s, and $h = 0.7$ m). $H_{s,VLF}$ for resonance events on the inner reef flat ranged from 0.14 to 0.83 m and had a skewed distribution with a median at 0.33 m, which is high considering the limited water depth on the reef and the exceptionally long wave periods. Narrow-banded fore reef spectra (Figure 5b; green curve) suggest that resonance was preferably induced by swell-dominated offshore wave conditions.VLF energy at the inner reef flat was positively correlated to the incident wave groupiness factor [*List*, 1991] which is a consequence of narrow-bandedness (not shown). This finding is consistent with *Nakaza and Hino* [1991]. A cross-correlation analysis was performed, for an example, VLF resonance event that occurred during swell conditions with a significant wave height of $H_s = 1.5$ m (Figure 5c). The cross-reef pattern showed synchronous water surface movement across the reef flat, indicating that VLF waves were not progressive, but resonated at the fundamental mode. Repetition of the pattern in horizontal direction showed subsequent VLF oscillations with the alternation between negative (Figure 5c; blue) and positive (Figure 5c; red) bars showing that troughs followed crests and vice versa.

4.2. Progressive-Dissipative Waves

Of the observed VLF waves, 36.8% were progressive-dissipative (Figure 5d) and occurred when water depths were low, with the majority (93%) occurring with reef flat water depths < 0.5 m and during low tides ($\mu =$ MSL -0.4 m; $\sigma = 0.2$ m). When water depths are low, frictional dissipation acts to reduce VLF energy over the reef flat leaving little energy at the shoreline (Figure 5e), independent of the incoming wave energy. This is consistent with *Pomeroy et al*. [2012b] who showed VLF amplification decreased for lower h and/or higher friction. The progressive-dissipative nature of these waves is also illustrated by the mean positive

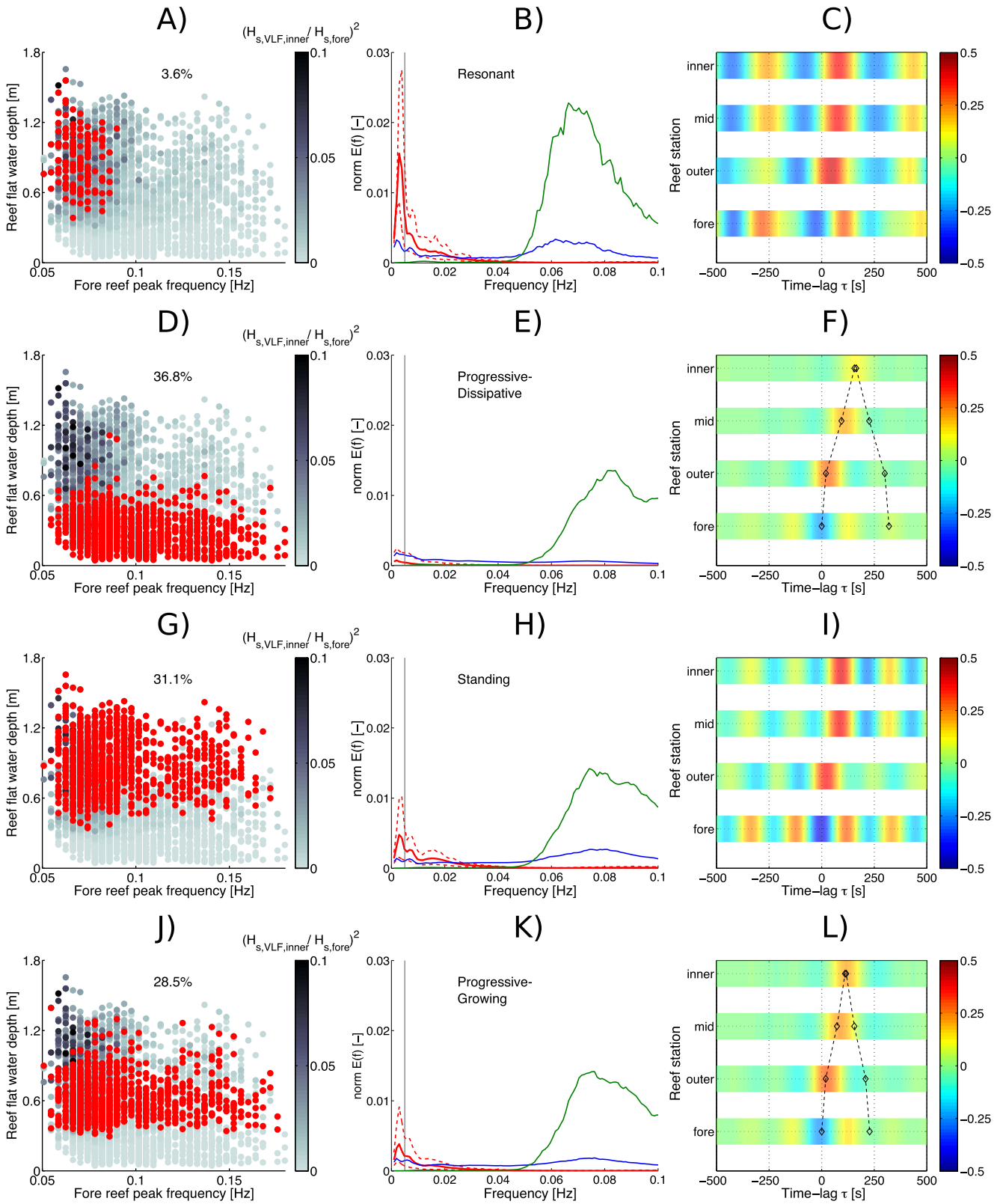
A)
B)
C)
D)
E)
F)
G)
H)
I)
J)
K)
L)
$(H_{s,VLF,inner}/H_{s,fore})^2$
3.6%
36.8%
31.1%
28.5%
Resonant
Progressive-Dissipative
Standing
Progressive-Growing
Reef flat water depth [m]
Fore reef peak frequency [Hz]
norm E(f) [–]
Frequency [Hz]
Reef station
inner
mid
outer
fore
Time–lag τ [s]

Figure 5.

correlation pattern for this class of wave, which follows the theoretical trajectory of a progressive wave and shows decreasing correlation toward the shoreline (Figure 5f). The theoretical progressive wave trajectory is calculated following *Janssen et al*. [2003] and is based on the celerity at the incident peak frequency ($f_{p,fore}$) and the local water depth. The switch from negative correlation at the fore reef (zero lag) to positive correlations on the reef flat is consistent with VLF wave generation by the breakpoint mechanism [*Pomeroy et al*., 2012a].

4.3. Standing Waves

VLF waves that showed increasing energy over the reef flat and included at least one standing harmonic constituted 31.1% of the observations (Figure 5g). These occurred with greater water depths on the reef flat ($h = 0.3$–1.7 m; $\mu = 0.9$ m; $\sigma = 0.2$ m), which enabled VLF waves to reflect at the shoreline and form standing waves. $H_{s,VLF}$ on the inner reef flat showed a skewed distribution with the median at 0.15 m, less than half the value of typical VLF resonance wave heights. However, one standing wave outlier with $H_{s,VLF} = 0.86$ m was observed (see also Figure 9b); we suspect that this anomalously large VLF standing wave is actually a resonant VLF wave that was not captured by our selection process. Sources of error in the identification of resonance events, particularly with regard to missing events, are discussed in section 5. For the standing wave class, the inner reef flat VLF energy band contained on average 1% of the total fore reef energy (Figure 5h). This is comparable to the average for the entire survey period (all classes combined). This suggests that as long as the forcing frequency is not similar to the eigen frequency of the reef flat, standing waves do not become resonant. We found that standing waves can exhibit a range of intensity in a wave signal, resulting in cross-correlation patterns that show both standing and progressive waves. For example, energetic incident waves ($H_s = 2.9$ m, $h = 1.3$ m) during the 2 March 2014 overwash event [*Quataert et al*., 2015; *Cheriton et al*., 2016] produced VLF waves that exhibited both progressive and weaker standing wave patterns, as seen at both positive and negative lags in the cross correlation (Figure 5i).

4.4. Progressive-Growing VLF Waves

For the remainder of the VLF wave events (28.5%; Figure 5j), VLF energy increased from the outer to the inner reef flat, but no resonant or standing wave harmonics were found; therefore, these VLF waves were classified as being progressive-growing. The progressive-growing VLF waves were associated with mid-range water depths on the reef flat, with the majority (92%) occurring with water depths between 0.4 and 1.0 m. Similar to the progressive-dissipative waves, these events occurred across a range of incident fore reef peak frequencies, showing no dependency with the offshore wave T_p (Figure 5j). Although both progressive-dissipative and progressive-growing waves had similar fore-reef spectra, the progressive-growing waves occurred with more HF energy at the outer reef flat due to higher offshore water levels ($\mu = \text{MSL} + 0.0$ m, $\sigma = 0.2$ m; compared to $\text{MSL} - 0.4$ m, $\sigma = 0.2$ m) (Figures 5e and 5k). Although this HF energy diminished by 95% toward the inner reef flat, the VLF wave energy increased by 86%, suggesting that breaking HF waves continued to transfer energy to the VLF band shoreward of the outer reef flat sensor, but the transfer was small (Figure 5k). The greater reef flat water depths enabled the progressive-growing VLF waves to propagate across the reef flat with a faster phase speed than the progressive-dissipative VLF waves, as indicated by the positive correlation bars that occur with shorter time-lags across the reef (Figures 5f and 5l). Because VLF energy increases shoreward over the reef, the cross-correlation values are expected to increase as well. However, this pattern is not present because the correlations were averaged over many wave events, which displayed a range of propagation speeds.

Examination of cross correlations for individual VLF wave events in the progressive-growing class suggests that reflection off the shoreline rarely occurs. We attribute the lack of reflection to the nonlinear shape of these VLF waves. By visual inspection of the time series, the observed progressive-growing VLF waves appear in the form of nonlinear (long-period) bores (Figure 6) for 50–80% of the records. Steep bore fronts

Figure 5. Characterization of the different very low frequency (VLF) wave classes obtained from the selection process. (a, d, g, j) Normalized VLF energy $(H_{s,VLF,inner}/H_{s,fore})^2$ at the inner reef flat as function of the fore reef incident wave peak frequency and time-averaged and spatially averaged reef flat water depth. Normalized VLF energy levels are indicated by the gray color scale. VLF wave class distribution and percentage of occurrence are noted. (b, e, h, k) Normalized, ensemble-averaged inner (red) and outer (blue) reef flat and fore reef (green) spectra for the different VLF wave classes; 90% confidence limits are shown in red dashes for the inner reef flat spectrum. Energy is normalized by the total fore reef wave energy. The transition from the VLF to infragravity band is indicated by the vertical gray line. (c, f, i, l) Cross correlations between the fore reef envelope with the low-pass filtered VLF time series at each instrument for various time-lags. Negative correlations are represented in blue and positive correlations in red; the dashed black line marks the theoretical incoming and reflected wave trajectories. Figures 5f and 5l show class-averaged results, whereas Figures 5c and 5i show results for a representative burst. Averaging is not useful in the latter cases, since the standing/resonant frequencies differ between events and correlations would diffuse.

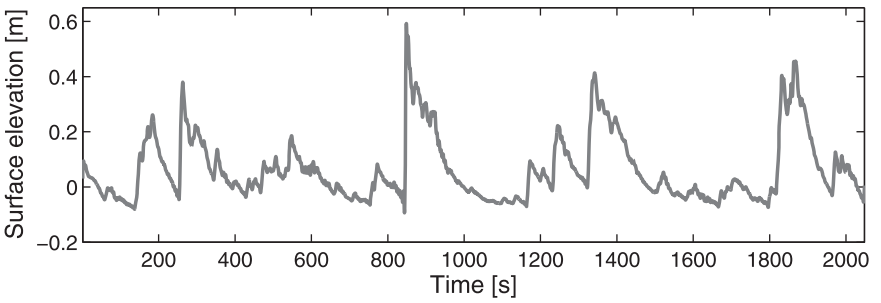

Figure 6. Example of a time series of water elevation from 19 February 2014 demonstrating an event classified as "Progressive-Growing" showing long-period, nonlinear bore waveforms. The bore starting at 850 s has a period of approximately 350 s.

and the lack of reflection suggest that most of the VLF wave energy is dissipated during the breaking process on the beach slope.

Our findings with respect to the occurrence of the different VLF wave classes are summarized in Table 1. As the water depth on the reef flat increases, more VLF wave energy reaches the shoreline and VLF waves start to reflect. Additionally, if the incoming HF periods are long, these VLF waves can be resonantly amplified. Thus, reef flat water depth and offshore wave period affect which class of VLF waves will occur over the reef flat.

5. Discussion

5.1. Sensitivity of Resonant Detection

By using the resonance diagram, we classified 3.6% of all VLF observations as resonant. However, this result is dependent on the choice of parameter values. One such parameter is the threshold value for the normalized energy ($normE_{p,transfer,thr}$). Events with energy above this threshold in the resonance diagram were defined to be resonant (Figure 4). This threshold was based on an optimization procedure that employed a Monte-Carlo simulation and measured the performance of different $normE_{p,transfer,thr}$ with respect to accuracy of the prediction and the number of selected resonant bursts. Since it is not known *a priori* which events were resonant, several assumptions were made. First, it was assumed that resonance is associated with the occurrence of highly energetic VLFs on the inner reef flat (Figure 5a). Subsequently, the top 5% most energetic VLF wave events ($EV_{normE,5\%}$, with EV indicating "number of events") were treated as events with a high *potential* of being resonant. With these reference cases, we then verified the accuracy (Acc) of our prediction. The events in the peak of the resonance diagram (Figure 4), $EV_{res,diagram}$ that were also within this top 5% energy category, were treated as "correct" predictions: $EV_{res,correct} = EV_{res,diagram} \cap EV_{normE,5\%}$.The accuracy, Acc, of the prediction was defined as the ratio between the correct and the total number of identified resonance events: $Acc = EV_{res,correct}/EV_{res,diagram}$. Then, we determined Rec—the "recognized" resonance events—which is an estimate of how many of the potential events were correctly recognized: $Rec = EV_{res,correct}/EV_{normE,5\%}$.

A Monte-Carlo simulation for a range of threshold values $normE_{p,transfer,thr}$ in the resonance diagram revealed that the optimal compromise between accuracy and the number of recognized events ($Acc^* Rec$) was found for $normE_{p,transfer,thr} = 0.0477$ (Figure 7). This threshold value is tailored specifically to our data set. While the data set-specific nature of this method is a drawback, we found it to produce significantly more accurate identifications of resonance. Here, the associated accuracy of the prediction was $Acc = 63\%$ and the number of recognized events $Rec = 46\%$. For comparison, we also evaluated the accuracy of identifying resonance through the application of the amplification, phase, and coherence criteria [*Pomeroy et al.*, 2012b]. Using this "three criteria

Table 1. Summary of the Occurrence of Very Low Frequency (VLF) Wave Classes

		Conditions	
Very Low Frequency Classes	Observed (%)	Reef Flat Water Depth h (m) for Majority of Events (>90%)	T_p (s)
Resonance	3.6	>0.5	>11
Standing	31.1	>0.5	
Progressive-growing	28.5	0.4–1.0	
Progressive-dissipative	36.8	<0.5	

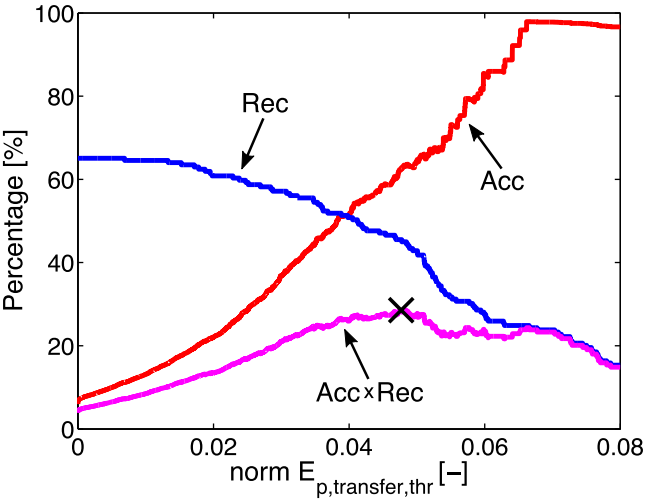

Figure 7. Optimization of the threshold $normE_{p,transfer,thr}$ value, based on a Monte Carlo simulation with 50,000 trials for the range $normE_{p,transfer,thr} = 0.00–0.08$. Shown are: the accuracy of the prediction, defined as $Acc = EV_{res,correct}/EV_{res,diagram}$ where $EV_{res,correct} = EV_{res,diagram} \cap EV_{normE,5\%}$ (red); indication for recognized resonant events $Rec = EV_{res,correct}/EV_{normE,5\%}$ (blue); a curve *Acc*Rec* (magenta) indicating the position of the optimal value for the threshold ("cross").

method," the same scoring system gives $Acc = 10\%$ and $Rec = 70\%$, indicating a tenfold increase in positive identifications. We argue that the reason for this increase is that many of these identified events are, in fact, standing waves. These false positives reduce the accuracy compared to the resonance diagram, and the *Rec* percentage is higher only because there is statistically more overlap with energetic events. Therefore, we find that the resonance diagram method is more suited for the detection of low-frequency wave resonance over reef flat environments. In addition, the peak transfer values, $H_{Ay}(f_{p,transfer})$, of the resulting $EV_{res,diagram}$ ranged from 0.63 to 3.40, showing that transfer function values under resonance conditions could be lower than the values found by *Péquignet et al*. [2009] and *Pomeroy et al*. [2012b]. Finally, we hypothesize that for larger data sets the resonance diagram becomes smoother and may be used to estimate the amount of damping in the reef system. This could be achieved by finding the half-power frequencies from the diagram and subsequently calculating the quality factor for damped seiching [see *Rabinovich*, 2009, equation 9.23].

Though the resonance diagram method greatly improves the accuracy of identifying resonance events, this method also has several drawbacks. As previously mentioned, the threshold value is selected based on specific aspects of a given data set. In addition, the resonance diagram method is a data postprocessing tool, which means that resonance predictions are based on existing data. These data are ideally in situ observations but in the absence of these, the data could be generated by a process-based model, given the offshore forcing and the local reef geometry.

We finally note that for each identified occurrence of VLF wave resonance, the resonance did not necessarily persist throughout the entire burst length. The duration of these resonance events can be short lived (Figure 8a). However, to evaluate the variations in resonance duration, longer measurement bursts would be needed.

5.2. Shape of Resonant VLF Waves

Because resonantly amplified VLF bores are associated with high propagation speeds and long periods, they have been mistaken for tsunamis; therefore, capturing their presence is important for coastal risk assessment [*Roeber and Bricker*, 2015]. Our field observations (Figure 8a), coupled with reports by others [*Nakaza and Hino*, 1991] confirm that resonant VLF waves can appear in bore-like shapes at the shoreline. However, it may be hard to characterize these nonlinear waveforms using conventional signal decomposition. A weakness of the Fast Fourier Transformation (FFT) method is that higher-frequency components would have to be included to approximate the almost vertical bore front. For bichromatic laboratory waves this can be done by retaining the higher harmonics of the low-frequency waves [*Van Dongeren et al*., 2007], but this is not possible for irregular waves. Instead, we found that a better characterization of the water surface motion could be achieved by employing a Hilbert-Huang Transformation (HHT) for the decomposition of the surface elevation time series [*Huang et al*., 1998; *Huang and Wu*, 2008; *Wu and Huang*, 2009]. This adaptive analysis technique is still in development, but has been used in several cases for hydrodynamic research [e.g., *Veltcheva*, 2002; *Dätig and Schlurmann*, 2004; *Ortega and Smith*, 2009]. The HHT decomposes a signal into 10–15 natural components, called Intrinsic Mode Functions (IMFs), which can vary in frequency and amplitude different from the preset harmonics of an FFT.

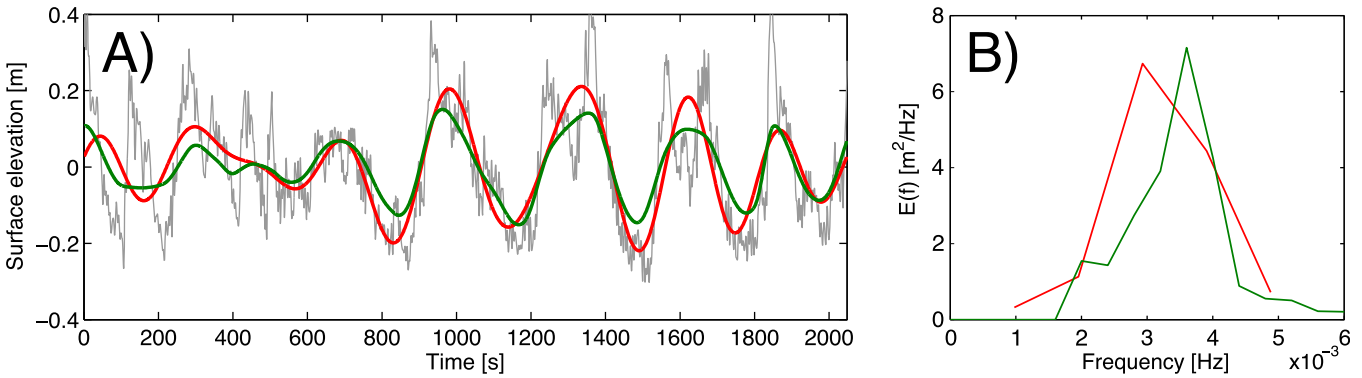

Figure 8. Comparison of the application of the Fast Fourier Transform (FFT) and the Hilbert-Huang Transform (HHT) methods to identify very low frequency (VLF) motions. (a) Time series of measured surface elevation (gray), VLF signal obtained by FFT (red), and by HHT (green). Sawtooth-shaped bore fronts are visible during the times of 900–1200 and 1800–2000 s. In contrast to the FFT method, these waveforms are identified by the HHT method. (b) Energy spectra of the VLF signal obtained using the FFT method (red) and the HHT method (green). The shifted peak in the HHT spectrum is caused by sharper transitions in the VLF wave shapes combined with the shorter-period oscillations preceding the resonant series at 0–600 s.

Here we present a brief description of our application of the HHT method; specific details of the HHT procedure can be found in *Huang et al.* [1998]. To obtain a robust estimate of the IMFs, we apply a variant of the HHT that is based on an ensemble empirical mode decomposition (EEMD) that minimizes mode mixing between IMFs [*Wu and Huang*, 2009]. The EEMD process is optimized by an end-effect correction as proposed by *Huang et al.* [1998] and employs a Piecewise Cubic Hermite Interpolating Polynomial for an accurate mode shape approximation. Energy spectra are obtained by applying a Hilbert transform to each IMF, which then gives a time series of frequencies and associated amplitudes. Summing the amplitudes for a predefined discrete frequency interval results in a so-called marginal spectrum. In this case, the amplitudes were first squared and subsequently halved, to acquire the associated (marginal) energy spectrum.

A single IMF describes the VLF wave resonance signal (Figure 8a), in accordance with *Huang et al.* [1998] who first proposed the association of IMFs with intrinsic physical signals. Moreover, the HHT approach captures the asymmetric waveform (Figure 8a). The associated (marginal) energy spectrum (Figure 8b) can be interpreted as a statistical measure for energy at a certain frequency. The analysis demonstrates that the HHT method has potential for investigations into irregular or bore-like waveforms in field data and therefore may particularly be valuable for detecting and understanding the deformation of resonant VLFs. We note that in contrast to VLF bores occurring within the progressive-growing class, VLF bores within the resonant class can grow much larger as was shown by *Roeber and Bricker* [2015] (see also Figures 5b, 5k, and 9). These resonantly amplified bores may contribute to flooding and have implications for coastal risk.

Also with respect to resonance events of short duration, a HHT is advantageous: instantaneous frequencies are determined by local derivatives of the phase, which results in greater frequency resolution compared to a spectrum acquired from FFT analysis, and, therefore, the spectra require less smoothing. Hence, the HHT method is also suited to investigate VLF motion in short time-records and thereby useful for analyses on short-lived resonance. However, one disadvantage of the HHT with our specific application is that it was computationally much more expensive compared to an FFT. It was therefore not performed for the entire classification of VLF waves in section 4, but only for a few selected bursts to demonstrate its use and potential for future research.

5.3. The Relation Between VLF Waves and Flooding

VLF motions cause a water level increase at the shoreline which is characterized by the inner VLF wave height $H_{s,VLF,inner}$. The magnitude of this wave height is dependent on the VLF class which is determined by the water depth on the reef and the incident wave peak period (Figure 5 and Table 1), but also by the offshore incident wave height $H_{s,fore}$ (Figure 9).

Different classes of VLF waves can occur across a range of $H_{s,fore}$, with larger incident wave heights resulting in larger $H_{s,VLF,inner}$. The slope of this dependency increases from progressive-dissipative waves to resonant waves (Figures 9a–9d). The slopes for the progressive-dissipative and progressive-growing classes are less steep because of the small water depths in which case there is higher dissipation (Figure 5). For the

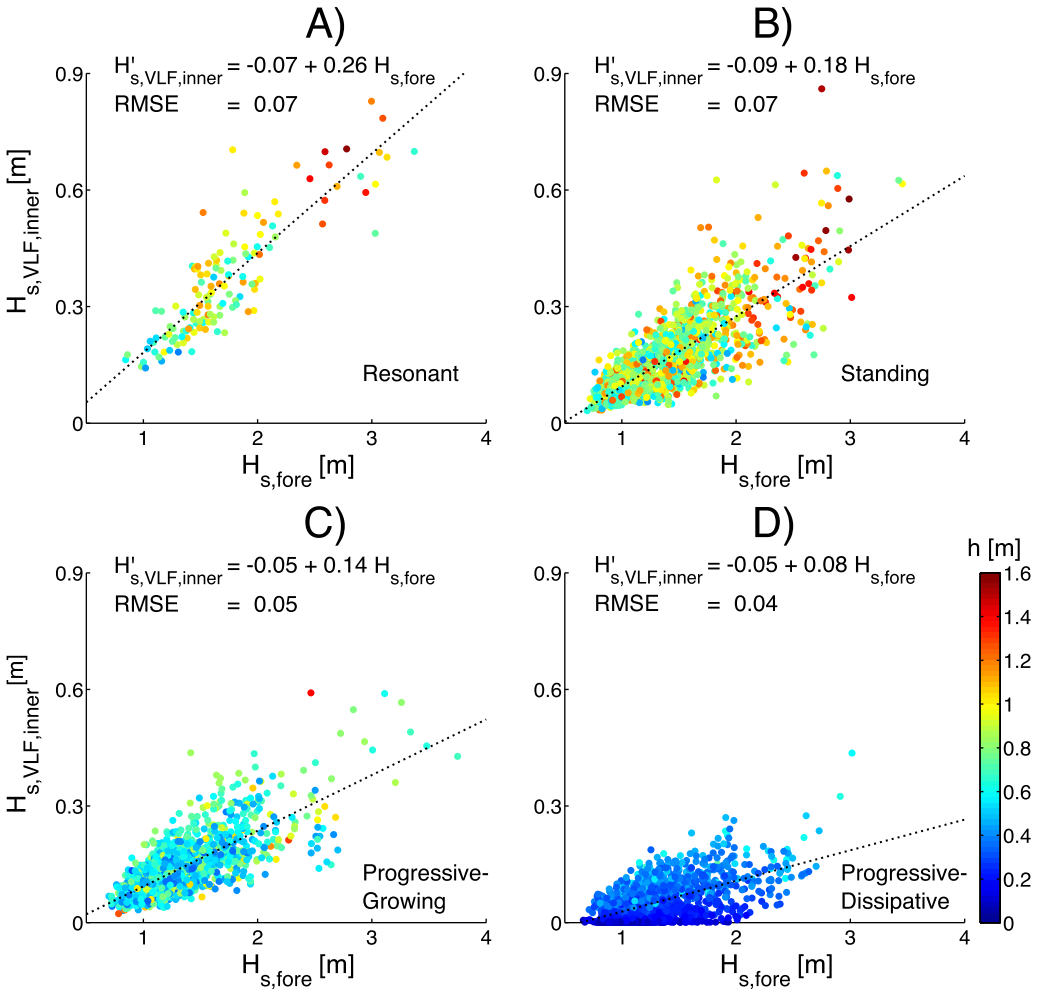

Figure 9. For each of the very low frequency (VLF) wave classes, the response of the inner reef flat VLF wave height ($H_{s,VLF,inner}$) to the offshore incident wave height ($H_{s,fore}$), colored by reef flat water depth (h). (a) Resonant, (b) standing, (c) progressive-growing, and (d) progressive-dissipative. In each plot, the slope of the point cloud trends ($H'_{s,VLF,inner}$) is indicated by a dotted line, with the linear fit and the root-mean-squared error (RMSE) indicated in the top left. $H'_{s,VLF,inner}$ is steepest for the resonant VLF waves (Figure 9a), indicating that for a given incident wave height, this class results in the largest VLF wave heights at the inner reef flat. The wave classes are also highly dependent on water depths, with larger water depths required for (a) resonant and (b) standing VLF waves, (c) mid-range depths for progressive-growing, and (d) the progressive-dissipative VLF waves occurring at the smallest water depths. This is consistent with greater dissipation occurring with smaller water depths, as demonstrated in Figure 5.

standing and resonant classes, the water depths are higher and the waves are much less affected by dissipation. Additionally, the efficient energy transfer in the case of resonance causes the largest slope.

To examine the role of the different VLF wave classes in flooding and runup, we examined two overwash events that occurred on Roi-Namur during the period of data collection, on 19 December 2013 and 2–3 March 2014 (Figure 10). Both events occurred under resonance-favoring conditions (T_p = 14–18 s, $h > 0.5$ m for more than 90% of the records) and (incident-band) wave heights up to 3.3 and 3.8 m, for December and March events, respectively. Since flooding was only witnessed during daylight hours [*Cheriton et al.*, 2016], a time frame of 24 h was chosen to establish wave class statistics for both events. During the two events, there was an order of magnitude higher occurrence of resonance (Figure 10a) compared to nonevent periods, which agrees with findings by *Cheriton et al.* [2016]. However, we note that the % occurrence of resonance found here (December 17%; March 33%) differs from that reported by *Cheriton et al.* [2016] (December 35%; March 44%) due to a difference in methods: we only considered the zeroth mode, used the mid-reef instead of the outer-reef station for the detection of standing waves, and chose a different approach from the "three criteria method" [*Pomeroy et al.*, 2012a,b] for identifying resonance. The higher %

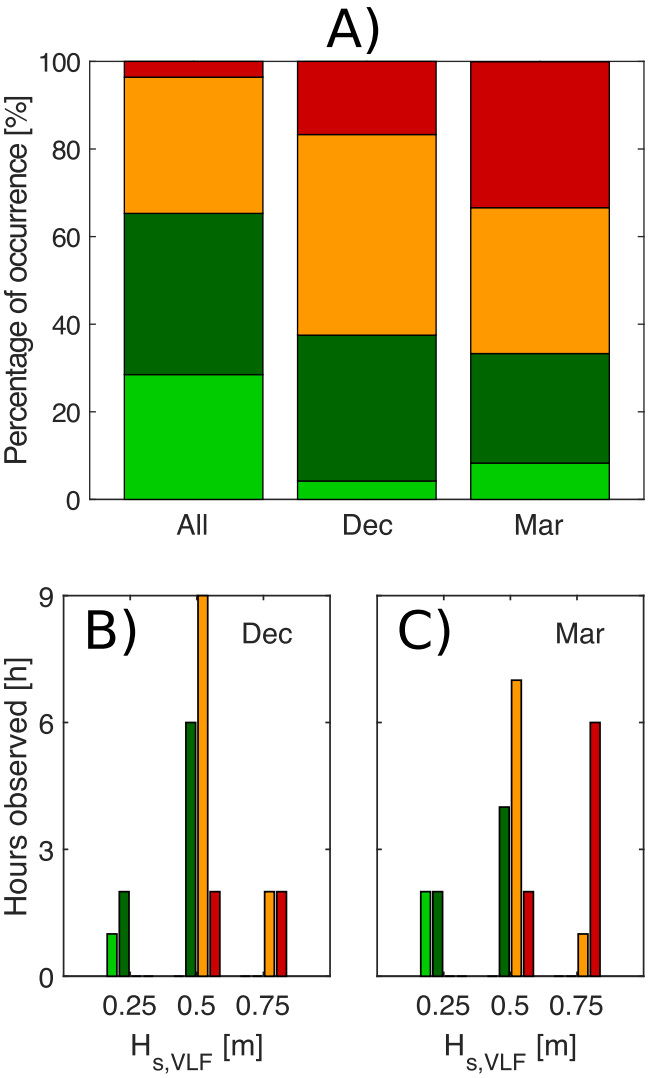

Figure 10. Percentage occurrence of the very low frequency (VLF) wave classes: resonant (red), standing (orange) progressive-growing (dark green), and progressive-dissipative (light green) during 24 h of the 19 December 2013 and 2–3 March 2014 flooding events. (a) Distribution of the wave classes in the overall data ("All") versus the distributions during the December ("Dec") and March ("Mar") events. Bottom plots show the number of hours the wave classes were observed according to inner reef flat VLF wave heights ($H_{s,VLF,inner}$) for the (b) December and (c) March events.

occurrence of resonance found by *Cheriton et al.* [2016] is further evidence of the propensity of the "three criteria method" to produce false positives by misidentifying standing waves as resonance.

Marginal flooding occurred during the December 2013 event, in which the percentage of resonance was lower than during the March 2014 event when flooding was more widespread. Moreover, the majority of the largest $H_{s,VLF,inner}$ during these events were categorized as resonant (Figures 10b and 10c), a relationship that was also found for the entire data set (Figure 9). *Cheriton et al.* [2016] also identified two instances of anomalously high runup that occurred outside of the overwash events; we found that these runup events also coincided with high instances of resonance. Resonance appears to be a key element in causing flooding and high runup.

We expect this to be case as well for other smooth and narrow reefs, which are characteristic of Kwajalein Atoll where Roi-Namur is located. In that respect, predicting resonance conditions by means of large-scale forecast models might serve as an indicator/early warning for enhanced runup or even flooding at such reefs. For coral reefs that are not smooth and narrow-like Roi-Namur, the rate of occurrence and relative significance of each VLF wave class to overwash and flooding is likely to depend on geomorphological factors, such as the width of the reef flat, reef frictional characteristics, and the fore reef slope, as explored by *Quataert et al.* [2015]. For wider reefs, we expect resonance to occur in the case of large water depths over the reef, as per equation (1) [*Péquignet et al.*, 2009; *Pomeroy et al.*, 2012b]. The probability of resonance will be lower in the case of reefs with high friction, i.e., a well-developed, healthy coral coverage [*Pomeroy et al.*, 2012b; *Quataert et al.*, 2015]. However, climate change related sea level rise and coral reef degradation [*Hoegh-Guldberg*, 1999; *Pandolfi et al.*, 2011] may eventually also make these reefs vulnerable to resonance and thereby increase the risk of flooding at reef-lined coasts that are currently well protected [*Storlazzi et al.*, 2015].

6. Conclusions

Wave and water level data obtained from a 5 month deployment at Roi-Namur on Kwajalein Atoll in the Republic of the Marshall Islands were used to categorize very low frequency (VLF) waves into four classes. Resonant, standing, progressive-growing, and progressive-dissipative waves were found to occur 3.6%,

31.1%, 28.5%, and 36.8% of the records, respectively. Resonant conditions were detected using a resonance diagram, a method that combines energy transfer estimates between fore reef wave group envelopes and the VLF signal near the beach with open basin theory. We found this to be an improved method for identifying resonance in large data sets as it produced more accurate identifications of VLF resonance than the "three criteria method" [*Pomeroy et al.*, 2012b], by decreasing the number of standing waves falsely identified as resonant motions. Compared to the other three VLF wave classes, resonance has the greatest potential to drive coastal flooding and island overwash, because of the large resulting shoreline VLF amplitudes. In the case of resonance, the energy transfer from the incident wave groups offshore to VLF waves on the reef flat is, on average, 5 times larger than for the other VLF wave classes. In addition, VLF waves can appear as bore-like waveforms and can retain this shape for resonant cases, which suggests that these VLF resonant waves are likely to disproportionately impact the shoreline. Because of the irregular waveform, we found the VLF band-pass filtered time series obtained from an FFT to be limited in representing these bore-like waves, and the use of a Hilbert-Huang transformation (HHT) is proposed instead. This research demonstrates that understanding the classes of VLF waves on reef flats is important for assessing coastal flooding hazards.

Acknowledgments

This work was funded by the U.S. Department of Defense's Strategic Environmental Research and Development Program under Project RC-2334 ("The Impact of Sea-Level Rise and Climate Change on Department of Defense Installations on Atolls in the Pacific Ocean"), the U.S. Geological Survey's Pacific Coastal and Marine Science Center, and Deltares through the Deltares Strategic Research in the "Hydro- and morphodynamics during extreme events" program (1230002). Joshua Logan, Kurt Rosenberger, and Thomas Reiss (USGS) provided invaluable field and data support. We would like to thank the U.S. Army Garrison-Kwajalein Atoll (USAG-KA) for their overarching support of this project. We are grateful to Andrew Pomeroy of the University of Western Australia for providing his cross-correlation analysis scripts. Thanks to Joachim Gawehn for suggesting the use of a Hilbert Huang Transformation. Use of trademark names does not imply USGS endorsement of products. The USGS data sets presented herein can be obtained by sending a written request to the corresponding author.

References

Baldock, T. E. (2012), Dissipation of incident forced long waves in the surf zone-Implications for the concept of "bound" wave release at short wave breaking, *Coastal Eng.*, *60*, 276–285, doi:10.1016/j.coastaleng.2011.11.002.

Battjes, J. A., H. J. Bakkenes, T. T. Janssen, and A. R. Van Dongeren (2004), Shoaling of subharmonic gravity waves, *J. Geophys. Res.*, *109*, C02009, doi:10.1029/2003JC001863.

Becker, J. M., M. A. Merrifield, and M. Ford (2014), Water level effects on breaking wave setup for Pacific Island fringing reefs, *J. Geophys. Res. Oceans*, *119*, 914–932, doi:10.1002/2013JC009373.

Cheriton, O. M., C. D. Storlazzi, and K. J. Rosenberger (2016), Observations of wave transformation over a fringing coral reef and the importance of low frequency waves and offshore water levels to runup, overwash, and coastal flooding, *J. Geophys. Res. Oceans*, *121*, 3121–3140, doi:10.1002/2015JC011231.

Dätig, M., and T. Schlurmann (2004), Performance and limitations of the Hilbert–Huang transformation (HHT) with an application to irregular water waves, *Ocean Eng.*, *31*(14-15), 1783–1834, doi:10.1016/j.oceaneng.2004.03.007.

Dean, R. G., and R. A. Dalrymple (1991), *Water Wave Mechanics for Engineers and Scientists, Adv. Ser. Ocean Eng.*, vol. 2, World Sci., Singapore.

Emery, W. J., and R. E. Thomson (2001), *Data Analysis Methods in Physical Oceanography*, Elsevier, Amsterdam, doi:10.1016/B978-044450756-3/50006-X.

Ferrario, F., M. W. Beck, C. D. Storlazzi, F. Micheli, C. C. Shepard, and L. Airoldi (2014), The effectiveness of coral reefs for coastal hazard risk reduction and adaptation, *Nat. Commun.*, *5*, 1–9, doi:10.1038/ncomms4794.

Fofonoff, N. P., and R. C. Millard (1983), Algorithms for computation of fundamental properties of seawater, *Q. J. Modern Foreign Lit.*, *44*, 53.

Gerritsen, F. (1980), Wave attenuation and wave set-up on a coastal reef, in *Proceedings of 17th International Conference on Coastal Engineering*, pp. 444–461, ASCE, Reston, Va.

Gourlay, M. R. (1996a), Wave set-up on coral reefs. 1. Set-up and wave-generated flow on an idealised two dimensional horizontal reef, *Coastal Eng.*, *27*(3-4), 161–193, doi:10.1016/0378-3839(96)00008-7.

Gourlay, M. R. (1996b), Wave set-up on coral reefs. 2. Set-up on reefs with various profiles, *Coastal Eng.*, *28*(1-4), 17–55, doi:10.1016/0378-3839(96)00009-9.

Hardy, T. A., and I. R. Young (1991), Modelling spectral wave transformation on a coral reef flat, in *Coastal Engineering—Climate for Change: Proceedings of 10th Australasian Conference on Coastal and Ocean Engineering*, Auckland, New Zealand, DSIR Marine and Freshwater, Water Quality Center, pp. 345–350.

Hardy, T. A., and I. R. Young (1996), Field study of wave attenuation on an offshore coral reef, *J. Geophys. Res.*, *101*(C6), 14,311–14,326, doi:10.1029/96JC00202.

Harkins, G. S., and M. J. Briggs (1994), Resonant forcing of harbors by infragravity waves, paper presented at Proceedings of the 24th International Conference on Coastal Engineering. Part 1 (of 3), October 23, 1994 - October 28, 1994, pp. 806–820, ASCE, Kobe, Japan.

Hench, J. L., J. J. Leichter, and S. G. Monismith (2008), Episodic circulation and exchange in a wave-driven coral reef and lagoon system, *Limnol. Oceanogr.*, *53*(6), 2681–2694, doi:10.4319/lo.2008.53.6.2681.

Hoegh-Guldberg, O. (1999), Climate change, coral bleaching and the future of the world's coral reefs, *Mar. Freshwater Res.*, *50*(8), 839–866, doi:10.1071/MF00030.

Hoeke, R. K., K. L. McInnes, J. C. Kruger, R. J. McNaught, J. R. Hunter, and S. G. Smithers (2013), Widespread inundation of Pacific islands triggered by distant-source wind-waves, *Global Planet. Change*, *108*, 128–138, doi:10.1016/j.gloplacha.2013.06.006.

Huang, N. E., and Z. Wu (2008), A review on Hilbert-Huang Transform: Method and its applications to geophysical studies, *Rev. Geophys.*, *46*, RG2006, doi:10.1029/2007RG000228.

Huang, N. E., Z. Shen, S. R. Long, M. C. Wu, H. H. Shih, Q. Zheng, N. C. Yen, C. C. Tung, and H. H. Liu (1998), The empirical mode decomposition and the Hilbert spectrum for nonlinear and non-stationary time series analysis, *Proc. Math. Phys. Eng. Sci.*, 903–995, doi:10.1098/rspa.1998.0193.

Jaffe, B. E., and B. M. Richmond (1992), Overwash variability on the shoreline of Guam during Typhoon Russ, in *Proceedings of 7th International Coral Reef Symposium*, vol. 1, pp. 257–264, University of Guam Press, UOG Station, Guam.

Janssen, T. T., J. A. Battjes, and A. R. Van Dongeren (2003), Long waves induced by short-wave groups over a sloping bottom, *J. Geophys. Res.*, *108*(C8), 3252, doi:10.1029/2002JC001515.

Kennedy, A. B., N. Mori, Y. Zhang, T. Yasuda, S.-E. Chen, Y. Tajima, W. Pecor, and K. Toride (2016), Observations and modeling of coastal Boulder transport and loading during super typhoon Haiyan, *Coastal Eng. J.*, *58*(1), 1640004, doi:10.1142/S0578563416400040.

List, J. H. (1991), Wave groupiness variations in the nearshore, *Coastal Eng.*, *15*(5-6), 475–496, doi:10.1016/0378-3839(91)90024-B.

Longuet-Higgins, M. S., and R. W. Stewart (1964), Radiation stresses in water waves: A physical discussion, with applications, *Deep Sea Res. Oceanogr. Abst.*, *11*(4), 529–562, doi:10.1016/0011-7471(64)90001-4.
Lowe, R. J., J. L. Falter, M. D. Bandet, G. Pawlak, M. J. Atkinson, S. G. Monismith, and J. R. Koseff (2005), Spectral wave dissipation over a barrier reef, *J. Geophys. Res.*, *110*, C04001, doi:10.1029/2004JC002711.
Lugo-Fernández, A., H. H. Roberts, W. J. Wiseman, and B. L. Carter (1998), Water level and currents of tidal and infragravity periods at Tague Reef, St. Croix (USVI), *Coral Reefs*, *17*(4), 343–349, doi:10.1007/s003380050137.
Merrifield, M. A., J. M. Becker, M. Ford, and Y. Yao (2014), Observations and estimates of wave-driven water level extremes at the Marshall Islands, *Geophys. Res. Lett.*, *41*, 7245–7253, doi:10.1002/2014GL061005.
Munk, W. H., and M. C. Sargent (1948), Adjustment of Bikini Atoll to ocean waves, *Trans. AGU*, *29*, 855–860.
Nakaza, E., and M. Hino (1991), Bore-like surf beat in a reef zone caused by wave groups of incident short period waves, *Fluid Dyn. Res.*, *7*(2), 89–100, doi:10.1016/0169-5983(91)90062-N.
Nakaza, E., S. Tsukayama, and M. Hino (1990), Bore-like surf beat on reef coasts, Proc. 22nd International Conference on Coastal Engineering, pp. 743–756, Delft, Netherlands. [Available at http://journals.tdl.org/icce/index.php/icce/article/viewArticle/4486.]
Nwogu, O., and Z. Demirbilek (2010), Infragravity wave motions and runup over shallow fringing reefs, *J. Waterw. Port Coastal Ocean Eng.*, *136*, 295–305, doi:10.1061/(ASCE)WW.1943-5460.0000050.
Ortega, J., and G. H. Smith (2009), Hilbert-Huang transform analysis of storm waves, *Appl. Ocean Res.*, *31*(3), 212–219, doi:10.1016/j.apor.2009.09.003.
Pandolfi, J. M., S. R. Connolly, D. J. Marshall, and A. L. Cohen (2011), Projecting coral reef futures under global warming and ocean acidification, *Science*, *333*(6041), 418–422, doi:10.1126/science.1204794.
Péquignet, A. C. N., J. M. Becker, M. A. Merrifield, and J. Aucan (2009), Forcing of resonant modes on a fringing reef during tropical storm Man-Yi, *Geophys. Res. Lett.*, *36*, 20–23, doi:10.1029/2008GL036259.
Pistrika, A. K., and S. N. Jonkman (2009), Damage to residential buildings due to flooding of New Orleans after hurricane Katrina, *Nat. Hazards*, *54*, 413–434, doi:10.1007/s11069-009-9476-y.
Pomeroy, A., R. Lowe, G. Symonds, A. Van Dongeren, and C. Moore (2012a), The dynamics of infragravity wave transformation over a fringing reef, *J. Geophys. Res.*, *117*, C11022, doi:10.1029/2012JC008310.
Pomeroy, A. W. M., A. van Dongeren, R. J. Lowe, J. S. M. van Thiel de Vries, and J. A. Roelvink (2012b), Low frequency wave resonance in fringing reef environments, Proc. 33rd International Conference on Coastal Engineering, Santander, Spain, *1*(33), pp. 1–10, doi:10.9753/icce.v33.currents.25.
Quataert, E., C. Storlazzi, A. Rooijen, O. Cheriton, and A. Dongeren (2015), The influence of coral reefs and climate change on wave-driven flooding of tropical coastlines, *Geophys. Res. Lett.*, *42*, 6407–6415, doi:10.1002/2015GL064861.
Rabinovich, A. B. (2009), Seiches and harbour oscillations, in *Handbook of Coastal and Ocean Engineering*, pp. 193–236, World Scientific, Singapore.
Roeber, V., and J. D. Bricker (2015), Destructive tsunami- wave generated by surf beat over a coral reef during Typhoon Haiyan, *Nat. Commun.*, *6*, 7854, doi:10.1038/ncomms8854.
Seelig, W. N. (1983), Laboratory study of reef-lagoon system hydraulics, *J. Waterw. Port Coastal Eng.*, *109*(4), 380–391, doi:10.1061/(ASCE)0733-950X(1983)109:4(380).
Shimozono, T., Y. Tajima, A. B. Kennedy, H. Nobuoka, J. Sasaki, and S. Sato (2015), Combined infragravity wave and sea-swell runup over fringing reefs by super typhoon Haiyan, *J. Geophys. Res. Oceans*, *120*, 4463–4486, doi:10.1002/2015JC010760.
Storlazzi, C. D., E. P. L. Elias, and P. Berkowitz (2015), Many atolls may be uninhabitable within decades due to climate change, *Nat. Sci. Rep.*, *5*, 14546, doi:10.1038/srep14546.
Symonds, G., D. A. Huntley, and A. J. Bowen (1982), Two-dimensional surf beat: Long wave generation by a time-varying breakpoint, *J. Geophys. Res.*, *87*(C1), 492–498, doi:10.1029/JC087iC01p00492.
Terry, J. P., and A. C. Falkland (2011), Responses of atoll freshwater lenses to storm-surge overwash in the Northern Cook Islands, *Hydrogeol. J.*, *18*(3), 749–759, doi:10.1007/s10040-009-0544-x.
Van Dongeren, A., A. Reniers, J. Battjes, and I. Svendsen (2003), Numerical modeling of infragravity wave response during DELILAH, *J. Geophys. Res.*, *108*(C9), 3288, doi:10.1029/2002JC001332.
Van Dongeren, A., J. Battjes, T. Janssen, J. Van Noorloos, K. Steenhauer, G. Steenbergen, and A. Reniers (2007), Shoaling and shoreline dissipation of low-frequency waves, *J. Geophys. Res.*, *112*, C02011, doi:10.1029/2006JC003701.
Veltcheva, A. D. (2002), Wave and group transformation by a Hilbert spectrum, *Coastal Eng. J.*, *44*(04), 283–300, doi:10.1142/S057856340200055X.
Vetter, O., J. M. Becker, M. A. Merrifield, A. C. Pequignet, J. Aucan, S. J. Boc, and C. E. Pollock (2010), Wave setup over a Pacific Island fringing reef, *J. Geophys. Res.*, *115*, C12066, doi:10.1029/2010JC006455.
Wilson, B. W. (1953), The mechanism of seiches in Table Bay Harbor, Cape Town, *Coastal Eng. Proc.*, *1*(4), 4.
Wu, Z., and N. E. Huang (2009), Ensemble empirical mode decomposition: A noise assisted data analysis method, *Adv. Adaptive Data Anal.*, *1*(1), 1–41, doi:10.1142/S1793536909000047.
Young, I. R. (1989), Wave transformation over coral reefs, *J. Geophys. Res.*, *94*(C7), 9779–9789, doi:10.1029/JC094iC07p09779.